A review on near net shape hot isostatic pressing of metallic materials: For industrial applications

Bioprinting 36 (2023) e00310

Contents lists available at ScienceDirect

Bioprinting

journal homepage: www.sciencedirect.com/journal/bioprinting

3D bioprinted GelMA platform for the production of lung tumor spheroids

Simona Villata [a], Marta Canta [a], Désirée Baruffaldi [a], Ignazio Roppolo [a,b], Candido Fabrizio Pirri [a,b], Francesca Frascella [a,*]

[a] DISAT, PolitoBIOMed Lab, Politecnico di Torino, Corso Duca degli Abruzzi 24, 10129, Turin, Italy
[b] Center for Sustainable Future Technologies, Italian Institute of Technology (IIT), Via Livorno 60, 10144, Turin, Italy

ARTICLE INFO

Keywords:
Spheroids
Lung cancer
3D bioprinting
GelMA

ABSTRACT

The study proposes a platform for the formation and culture of non-small cell lung cancer (NSCLC) spheroids, to obtain an *in vitro* model suitable for drug and therapy testing. To achieve that, traditional cell culture is compared to methacrylated gelatin (GelMA) 3D bioprinting, in order to explore not only the potential of the matrix itself, but also the impact of different architectures on spheroid formation. Starting from a systematic analysis, where GelMA concentration, methacrylation degree and cell seeding concentration is set; three different architectures (round, ring and grid) are analyzed in terms of spheroid formation and growth, using 3D bioprinting. The study reveals that Very High GelMA 7.5% w/v formulation, with single cells dispersed in, is the best bioink to obtain NSCLC spheroids. Moreover, grid architecture performs in the best way, because of the highest volume-surface area ratio. The designed GelMA platform can be used as a powerful *in vitro* tool for drug testing and therapy screening, that can be designed playing with four different parameters: cell concentration, GelMA methacrylation degree, GelMA concentration and geometry.

1. Introduction

Lung cancer is one of the most common tumors worldwide, next to prostate cancer in men and breast cancer in women (American Cancer Society https://www.cancer.org/). The American Cancer Society's estimate about 240,000 new cases of lung cancer in the United States for 2022, and about 130,000 deaths from lung cancer in the same year. There are different types of lung cancer, which can be divided into two groups according to histological and molecular features: small and non-small cell lung cancer. Specifically, non-small cell lung cancer (NSCLC) accounts for 80% of total diagnosis. It consists of several subtypes which are adenocarcinoma (32–40%), squamous cells (25–30%) and large cells (8–16%) carcinoma [1] Nowadays; as a result of research efforts, many therapeutic protocols are available for lung cancer treatments [2] but, unfortunately, the insurgence of drug resistance and metastasis formation usually leads to patients death [3,4]. In the last years, *in vivo* and *in vitro* models have been optimized as platforms for drug and therapy testing. Those can be summarized in: *in vivo* animal models [5,6], traditional 2D culture systems [7] and 3D ones, i.e. scaffolds [8,9], spheroids [10–14] and organoids [15–18]. In addition, 3D bioprinting techniques recently emerged as powerful technique to manufacture living tissues and organs, including of vascularized constructs [19,20]. In this investigation, spheroids were considered as model, to overcome the limitation of 2D cell culture, that oversimplifies the natural 3D *in vivo* environment [21]. Moreover, spheroids allow to limit the use of *in vivo* animal models, following the 3R principle of Russel and Burch, i.e. Replacement, Reduction and Refinement [22]. Spheroids are micro-tumors, in particular they are cell aggregates organized in a spherical shape in which cell-to-cell interactions are promoted. This self-assembled 3D cell culture are characterized by a diameter starting from about 100 μm [23]. Usually, a spheroid shows three different concentric zones related to the availability of oxygen and nutrients: an external one, in which cells are highly proliferating and migrating; a middle part where cells are quiescent, because of the lower amount of nutrients; and a necrotic zone, in which oxygen and nourishment are not sufficient to maintain high levels of cell viability [24]. Regarding spheroid size, Singh et al. [23] in 2020 highlighted the importance of tumor spheroid dimension in response to the drug treatment. In particular, they reported that spheroids of large dimensions (>400 μm of diameter) are not suitable for drug toxicity studies compared to spheroids of diameter approximately 150–350 μm that produce more reliable and reproducible data. Lately, spheroids have been also employed to study NSCLC. In particular, they were useful to analyze cell-to-cell adhesion, chemoresistance, tumor heterogeneity and extracellular

* Corresponding author.s
E-mail address: francesca.frascella@polito.it (F. Frascella).

https://doi.org/10.1016/j.bprint.2023.e00310
Received 14 June 2023; Received in revised form 15 September 2023; Accepted 22 September 2023
Available online 25 September 2023

matrix deposition [10]. Spheroids are commonly obtained employing two scaffold-free techniques: liquid overlay, which is based on the interruption of cell adhesion by using special non-adhesive substrates, and hanging drop, which takes advantages of surface tension and gravitational forces [12]. A drawback of these techniques is the absence of extracellular matrix, which can mimic the biomechanical properties of native tissue [25–27], in this case the tumor (that is usually stiffer than the healthy tissue) [28]. Consequently, in the last years, many investigations have been conducted on the formation of spheroids inside matrices to move towards more complex 3D models [28]. Matrigel, collagen and gelatin are used to establish spheroids-based cell culture, so to provide a microenvironment similar to the extracellular matrix for the cancer cell population [29]. Another crucial aspect is the possibility to act on the architecture of the model. In the last years, 3D bioprinted constructs [30,31] started to be considered as good candidates for spheroid culture. One promising bioink is methacrylated gelatin (GelMA) [32–36] a photo-crosslinkable hydrogel, broadly used as cell culture supporting matrix for a wide spectrum of applications [37,38]. The main properties of this material are its excellent biocompatibility, biodegradability, and printability. Moreover, GelMA can be used at different concentrations w/v% and synthesized with different degrees of methacrylation. This is really important from many points of view, as both concentration [25,39,40] and methacrylation degree [41] could impact on the mechanical properties of the material. This means that GelMA is a really tunable material and can be a great candidate to design an environment where cells can experience more *in vivo*-like mechanical conditions. This work aims to investigate different GelMA bioinks to support not only the culture of NSCLC spheroids, but also their formation from single cells [42]. Hence, GelMA bioinks were investigated at different degrees of methacrylation and concentrations and then 3D printed in three different architectures (round, ring and grid), to find the best conditions to set up a NSCLC spheroid *in vitro* model, that can be used for high throughput drug and therapy screening.

2. Material and Methods

2.1. GelMA synthesis

GelMa was synthesized following the protocol first reported by Van Den Bulcke et al. [43]. Briefly, 10 g type B gelatin from bovine skin (Sigma Aldrich) were dissolved into Dulbecco's Phosphate Buffered Saline (DPBS, Sigma) at a concentration of 10% w/v at 50 °C. To introduce methacrylic groups, Methacrylic Anhydride (MA, Sigma) was slowly added in different amounts (2 ml, 4 ml, 8 ml and 20 ml), according to the functionalization degree desired. Four different degrees of substitution were synthesized, indicated as Low, Medium, High and Very High respectively. The reaction lasted 2 h, then it was stopped diluting with an equal volume of DPBS. The resulting solution was dialyzed in dd-H_2O with cellulose membrane (12–14 kDa molecular weight cutoff, Sigma) for 1 week at 40 °C, to completely remove unreacted MA. Finally, GelMA was freeze-dried.

Formulations for cell culture support were obtained by dissolving the GelMA at different methacrylation degrees at different concentrations w/v (5%, 7.5%, 10%) in complete cell culture medium, previously combined with lithium phenyl-2,4,6-trimethylbenzoylphosphinate (LAP; 0.05% w/v final concentration) as photoinitiator at a concentration of 2.5 mg/ml. The solutions were heated at 60 °C for 1 h and filtered through 0.45 μm and 0.22 μm PES membrane filters (Asimo) to sterilize. GelMA was too viscous to be only filtered with 0.22 μm filter, so a previous step of 0.45 μm filtering was performed, in order to remove larger particulate. All GelMA solutions were pre-warmed at 37 °C before cells were added.

2.2. Degree of functionalization (DoF)

2.2.1. Fluoraldehyde assay

For the assessment of gelatin's degree of substitution of $–NH_2$ groups on gelatin (i.e DoF on lysine Lys residues), all GelMA formulations were dissolved in DPBS at the concentration of 2 mg/ml. Then, 300 μl of GelMA were mixed with 600 μl of fluoraldehyde o-phthalaldehyde (OPA) reagent solution. It reacts with primary amines of amino acids, peptides and proteins to enable fluorescent detection and quantification (ThermoFisher). Gelatin was used as positive control. After 1 min, fluorescence intensity (I) was read by using Synergy™ HTX Multi-Mode Microplate Reader (BioTek) at 450 nm (exc = 360 nm). DoF was then calculated as in **Equation (1)**.

$$\text{DoF on Lys} = [1-(I_{sample}-I_{blank})/(I_{control}-I_{blank})] \text{ x } 100 \quad (1)$$

Where I_{sample} was the fluorescence intensity of the GelMA solution of interest and $I_{control}$ was the intensity of gelatin solution at the same concentration. At the end, as Lys residues presence in the gelatine chain is 4% [44], the total DoF on Lys was obtained. Calculations and results are reported in the Supporting Information file.

2.2.2. ^1H NMR

As methacrylation reaction could also functionalize other amino acids in gelatine, H NMR experiments were also conducted to obtain the total degree of functionalization. 12 mg of each sample were dissolved in H_2O and spectra were recorded on a Bruker Advance 400 MHz at room temperature. Signals corresponding to the methylene protons of the methacrylate group appeared at 5.4–5.7 ppm. Quantification of MA content was done by integration of these protons taking as reference the signal at 7.15–7.4 ppm, corresponding to Phe aromatic protons (which remain unaltered along the chemical modification reactions) [45].

2.3. Cell culture

Human NSCLC cell lines, A549 and A549-GFP+ were kindly provided by Dr. Valentina Monica, Department of Oncology, University of Torino, AOU San Luigi Gonzaga. Specifically, A549 were infected to constitutively express histonic protein H2B fused with the green fluorescent protein (GFP). Both cell lines were cultured in Gibco BenchStable™ RPMI 1640 GlutaMAXTM medium (Thermo Fisher) supplemented with 10% Fetal Bovine Serum (Sigma Aldich) and 1% penicillin/streptomycin (Sigma Aldrich) in a humidified incubator at 37 °C, 5% CO_2. All cell lines were periodically checked for mycoplasma contamination.

2.4. Spheroids generation in 96 well plates

Prior to cell seeding, 96 well flat bottom plates (Greiner bio-one) were covered with 30 μl of the selected GelMA formulation and incubated for 2 min at 37 °C, 5% CO_2. Then, the plate surface was irradiated ($\lambda = 405$ nm, optic fiber LED light, $I = 10$ mW cm^{-2}) for 1 min, to induce GelMA photopolymerization.

After coating formation, A549 or A549-GFP + cells were suspended at different cell densities (10^3, 2×10^3, 4×10^3, 8×10^3 or 5×10^3, 1×10^4, 1.5×10^4 cells/50 μl, respectively) in the 37 °C pre-heated GelMA formulations and seeded onto the 96 well plate (50 μl/well). Immediately after seeding, the plates were irradiated ($\lambda = 365$ nm, Asiga® Flash Cure Box, $I = 10$ mW cm^{-2}) for 30 s to induce the cell laden GelMA photopolymerization. Then, 200 μl of cell culture medium were added to each well and replaced every 5 days, until the end of the experiment. Spheroid images were captured with Eclipse Ti2 Nikon microscope equipped with a Crest X-Light spinning disk, after 12 days of culture.

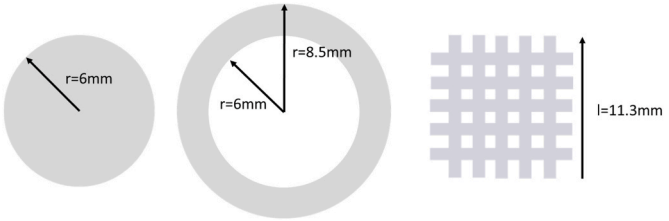

Scheme 1. Structures design, with corresponding dimensions.

2.5. Spheroids generation in bioprinted structures

To analyze how the construct geometry can affect spheroid formation, different architectures were produced with a 3D discovery bioprinter (RegenHu). Cell laden GelMA (1.5×10^4 cells/50 µl, so 3×10^6 cells/ml) was extruded using a 3 ml UV-secure pneumatic-driven extrusion printhead and a nozzle with an inner diameter of 250 µm, directly into 6 well suspension plates (Greiner bio-one). It was then photopolymerized. The feed rate was 15 mm/s and the printing pressure was approximately 0.080 MPa. G-codes were generated using BioCAD software (RegenHu). Three different architectures were generated: round, ring and grid, with the same volume in terms of cell laden GelMA, so to analyze the same starting conditions. Each geometry consisted of 4 layers, each one 500 µm thick. The samples were irradiated for 1 min (λ = 365 nm, Asiga® Flash Cure Box, I = 10 mW cm^{-2}). These photocrosslinking conditions were chosen because the tested samples showed high vitality in Live and Dead assay even after 12 days of culture, and long-term stability of the constructs: those are coherent with the results obtained from FT-IR experiments, indicating marginal presence of cytotoxic moieties.

The same amount of cell-laden GelMA was obtained designing the layers of the three structures with the same superficial area, i.e. 113 mm^2. For this reason, round structure has a radius of 6 mm, ring structure has an internal radius of 6 mm and an external radius of 8.5 mm and grid structure presents 10 lines, each one with thickness of 1 mm and length of 11.3 mm. Schematic representation of the designed layers is presented in Scheme 1.

After the photocrosslinking, the samples were then submerged in 5 ml complete cell culture medium and placed in an incubator at 37 °C and 5% CO_2. Cell culture medium was replaced every 5 days until the end of the experiments.

2.6. Material characterization

FT-IR spectra were collected using a ThermoScientific Nicolet iS50 FTIR spectrometer in ATR (Attenuated Total Reflection) configuration 64 scans were collected for each sample in the range of 4000–600 cm^{-1}, with a resolution of 2 cm^{-1}. Spectra were normalized taking as reference amide I absorption peak centered around 1635 cm^{-1}. To assess the degree of reaction of methacrylate double bonds, the decrease of the peak centered around 940 cm^{-1} (related to CH wagging in $CH{=}CH_2$ bonds [46,47]) was followed.

Morphological characterization of crosslinked GelMA hydrogels was carried out by field emission scanning electron microscopy (FESEM, Zeiss Supra 40). To prepare the samples, 50 µl of GelMA were poured into a 96 well plate and photopolymerized as previously described. Then, samples were incubated overnight with 200 µl of RPMI and lyophilized. Before characterization, the samples were coated with a film of Pt/Pd 5 nm thick. For the image analysis ImageJ (Java) software was employed.

3D bioprinted crosslinked GelMA structures were characterized in terms of printing fidelity. A 3D Scanner 3Shape E3 was used to carry out an evaluation of the fidelity and resolution of the 3D bioprinted architecture. Talc powder was used to enable the observation. The obtained digital file was then compared with the digital model to evaluate 3D printing fidelity.

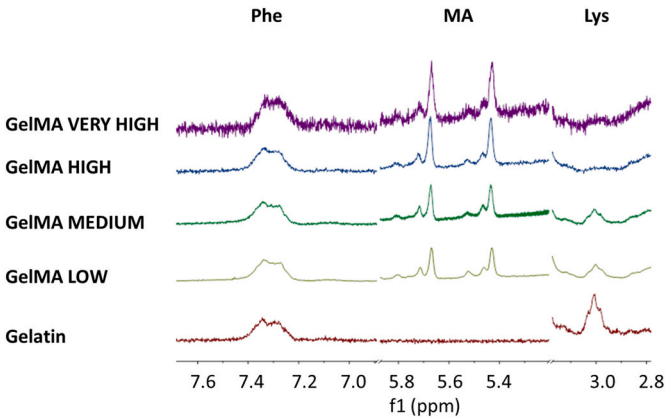

Fig. 1. Selected ^1H NMR spectral regions of gelatin and GelMA, and peak assignment for phenylalanine (Phe), methacrylate (MA and lysine (Lys) protons.

2.7. Cell metabolic activity

Resazurin assay (Sigma Aldrich) was performed on the bio printed architectures at 6 and 12 days of culture. To exclude the eventual contribution of the cells leakage from the printed structures, the 3D constructs were transferred in new well plates before starting the assay. Briefly, 500 µl of Resazurin (0.1 mg/ml in PBS) was added to each well and left in the incubator. After 4 h, the solution containing Resazurin (3 × 200 µl for each well) was transferred in 96 well white microplates (Corning). The fluorescence signal of the resazurin's reduced form, resorufin (exc/em: 530/590), which is proportional to the number of metabolic active cells, was detected by the SynergyTM HTX Multi-Mode Microplate Reader (BioTek). The signal resulting from the structures without cells was used as background. The differences between the technical replicates were then analyzed by two-way ANOVA.

LIVE/DEAD cell assay kit (Sigma Aldrich) was used to evaluate cell viability after 12 days of culture. In detail, the bioprinted samples were washed twice with DPBS, stained with 1.5 µM Propidium Iodide (PI) and 1 µM Calcein-AM for 30 min in an incubator at 37 °C and washed again with DPBS to remove the unreacted dyes. The fluorescence signals were detected using an Eclipse Ti2 Nikon (Tokyo, Japan) microscope equipped with a Crest X-Light spinning disk.

2.8. Spheroids image analysis

After 6 and 12 days of culture, the bioprinted samples were washed with DPBS, fixed with Paraformaldehyde, 4% (Alpha Aesar) for 1 h at room temperature (RT), washed again three times with DPBS and stored at 4 °C until staining. Each structure was stained with WGA Alexa Fluor® 647 conjugate (Thermo Fisher scientific) and DAPI (Sigma-Aldrich). In details, the samples were washed with DPBS and stained with 5 µg/ml WGA Alexa Fluor® 647 conjugate, for 1 h at RT. Then, samples were permeabilized with 0.25% Triton x-100 (Sigma-Aldrich) for 30 min at RT and stained with 0.4 mM DAPI for 3 h at RT. Fluorescent images were collected using an Eclipse Ti2 Nikon microscope equipped with a Crest X-Light spinning disk.

For the diameter analysis, at least five images for architecture (round, ring or grid), for each condition (GelMA 7.5% High and Very High) and time point (6 and 12 days) were analyzed by using the software ImageJ. The size distribution analysis was generated using the software tool. The diameters were obtained arithmetically and their distribution was expressed in terms of frequency (%) of each diameter in each geometry.

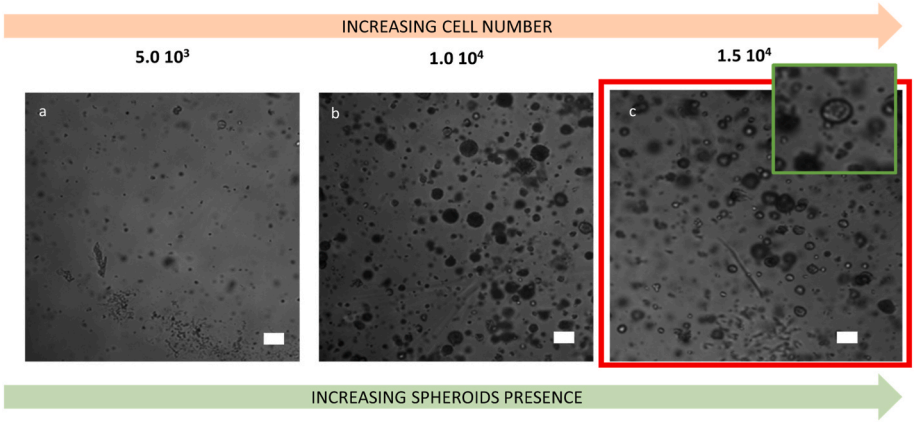

Fig. 2. Representative brightfield images of A549 seeded at different densities (5.0×10^3, 1.0×10^4,1.5×10^4 cells/50 µl) and cultured in crosslinked GelMA hydrogel for 12 days. Here, we reported as an example the GelMA 10% w/v with Medium degree of methacrylation. 4× magnification is provided in green squares. Scale bar: 100 µm.

3. Results

3.1. GelMA degree of functionalization determinated by ^1H NMR

As can be seen in Fig. 1, increasing the amount of MA added during the reaction, it is found a simultaneous decrease of the protons corresponding to Lys residue (signal at 3.0 ppm) and an increase of the methacrylate signals at 5.4–5.7 ppm.

The values obtained (2.1%, 2.5%, 3.1% and 4.1% w/w) were substantially similar to those determined by titration of amino groups (i.e. 2.5%, 2.8%, 3.1% and 3.9%, results showed in Fig. S1), which is in accordance to other author's findings [44]. This means that methacrylation reaction takes place almost exclusively onto primary amino groups of Lys, at least under the described experimental functionalization conditions.

3.2. Selection of GelMA formulation and A549 density for spheroids formation

A systematic analysis was conducted on A549 spheroid formation and growth in different crosslinked GelMA formulations and with different cell concentrations, to identify optimal conditions. The aim was a preliminary screening of the matrices to quick and easily select the most promising conditions, so to evaluate afterwards the behavior of the selected matrices in forming 3d bioprinted constructs. Indeed, mimicking of tumor microenvironment features is a crucial point in the development of an efficient 3D culture system. To test different conditions and be able to select the best one, DoF was modulated during

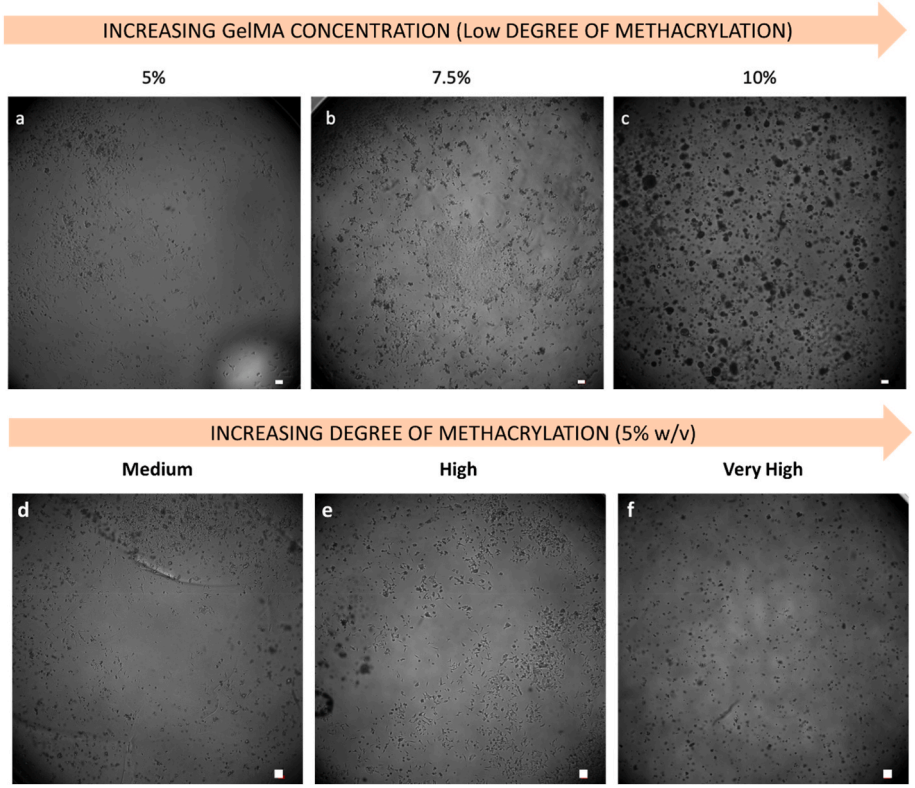

Fig. 3. Brightfield images of A549 cultured in not suitable conditions: GelMA Low formulations concentrated a) 5% w/v, b) 7.5% w/v and c) 10% w/v, GelMA Medium 5% w/v d), GelMA High 5% w/v e), GelMA Very High 5% w/v f). Scale bar: 100 µm.

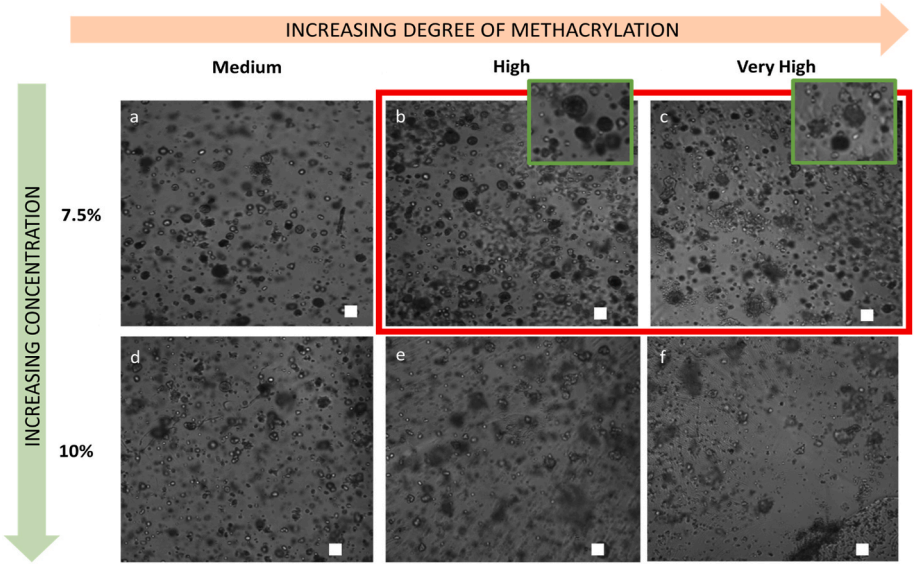

Fig. 4. Brightfield images of spheroids in different GelMA formulations. Scale bar: 100 μm. 4× magnification is provided in green squares.

GelMA synthesis. This modification also influences other parameters, like chain mobility and conformation [48], which ultimately can affect spheroid growth and invasion [49].

Furthermore, degree of conversion was evaluated by FT-IR, evidencing high conversion degree (>80%, Supporting Information, Fig. S2), not inducing cytotoxic effects.

3.2.1. *Selection of A549 density*

First of all, three seeding densities (5.0×10^3, 1.0×10^4, 1.5×10^4 cells/50 μl) were analyzed, leaving the cells growing in different crosslinked GelMA hydrogels, in terms of concentration and methacrylation degree for 12 days. A systematic analysis, based on brightfield images of each condition was performed. The optimal spheroids were identified as cell aggregates with a uniform morphology, a round shape and defined external boundaries. The spheroids should appear as a translucent ball, with a darker core and increasing dimensions [50]. During the analysis, the optimal GelMA formulation was selected as the one able to produce a lot of big cell aggregates. Fig. 2 shows some representative images of A549 spheroids. As already reported in a first concentration screening (Supporting Information, Fig. S2), in all GelMA tested there was a correlation between the initial cell seeding density and the spheroid formation. A clear difference was visible between 5.0×10^3 and 1.0×10^4 cells seeding densities, with a higher number of cell aggregates detected in the second one. The same behavior was not so evident, increasing densities to 1.5×10^4 cells, clearly suggesting that there was a threshold like trend. The selected cell starting concentration was 1.5×10^4 cells/50 μl (3×10^5 cells/ml), because it performed more homogeneously comparing the different GelMA methacrylation degrees and concentrations.

3.2.2. *Selection of GelMA*

The A549 spheroid formation, starting from the cell concentration of 1.5×10^4 cells/50 μl (3×10^5 cells/ml), was tested in different crosslinked GelMA solutions, varying both GelMA concentration (5, 7.5, 10% w/v) and methacrylation level (Low, Medium, High, Very High), starting from the cell concentration of 1.5×10^4 cells/50 μl (3×10^5 cells/ml). This investigation allows to assess the impact of these parameters on cell behavior. Comparing different gelatin concentrations for the same DoF, it was clear that only the highest one (Fig. 3 c) allowed the formation of cell aggregates, while in the lowest (Fig. 3 a and **b**), no spheroids were observed. Moreover, in all crosslinked GelMA Low formulations, cell sedimentation and adhesion to the bottom of the well plate was observed. The same phenomenon was observed for low concentration of GelMA, even if with a higher degree of functionalization (Fig. 3 d-f). This phenomenon can be related to the low crosslinking degree in hydrogels obtained using precursors with low methacrylation degree [48], or obtained from low concentrations of precursors. In both the cases cells showed a tendency to deposit and begin to grow in 2D. Consequently, all Low GelMA formulations and the 5% concentrations were excluded from further investigations.

Further investigations were made on GelMA 7.5% and 10% w/v, with Medium, High and Very High degree of methacrylation. The representative brightfield images acquired after 12 days of culture and depicted in Fig. 4, showed that all these crosslinked GelMA formulations allowed the formation of spheroids, even with differences between the samples. Interestingly, aggregate formation in 7.5% crosslinked GelMA increased with higher degree of methacrylation. In particular, High and Very High formulations (Fig. 4 b and **c**), showed a major extent of spheroids with a round cell morphology compared to Medium one (Fig. 4 a), in which many single cells or really small aggregates were more numerous. On the contrary, for what concerns the 10%v/w formulation, GelMA Medium (Fig. 4 d) appeared to be the best condition for spheroid formation, even if not comparable with GelMA 7.5% High and Very High (Fig. 4 b and **c**). Indeed, in crosslinked GelMA Medium 10%, many round cell aggregates appeared after 12 days, while in the High and Very High formulation at 10% w/v (Fig. 4 e and **f**), few round shape spheroids were detected and the majority of cells did not integrate in compact spheres. Furthermore, the images acquired for these last two formulations appeared less clear due to a loss of transparency of the matrix, making them unsuitable for microscopy analysis.

Even if further investigations are needed to fully explain these results, it is possible to speculate that the matrix methacrylation plays a driving role in matrix stiffness [41] and in spheroid formation. Indeed, as already reported in the literature [51,52], too rigid matrix makes spheroid expansion difficult, as well as hinders cell movements and aggregation. While, on the contrary, too soft matrix does not constrain the cells to grow in aggregates, promoting cell migration and allowing in some cases the sedimentation. Indeed, considering our results, the best GelMA formulation for spheroids formation are the ones whose properties promote cell confinement without limiting their proliferation and expansion. Therefore, the 7.5% High and Very High, that represent conditions between the lowest methacrylated (Medium 7.5% and 10%) and the highest methacrylated and concentrated formulations (High and Very High 10%) represented the election conditions.

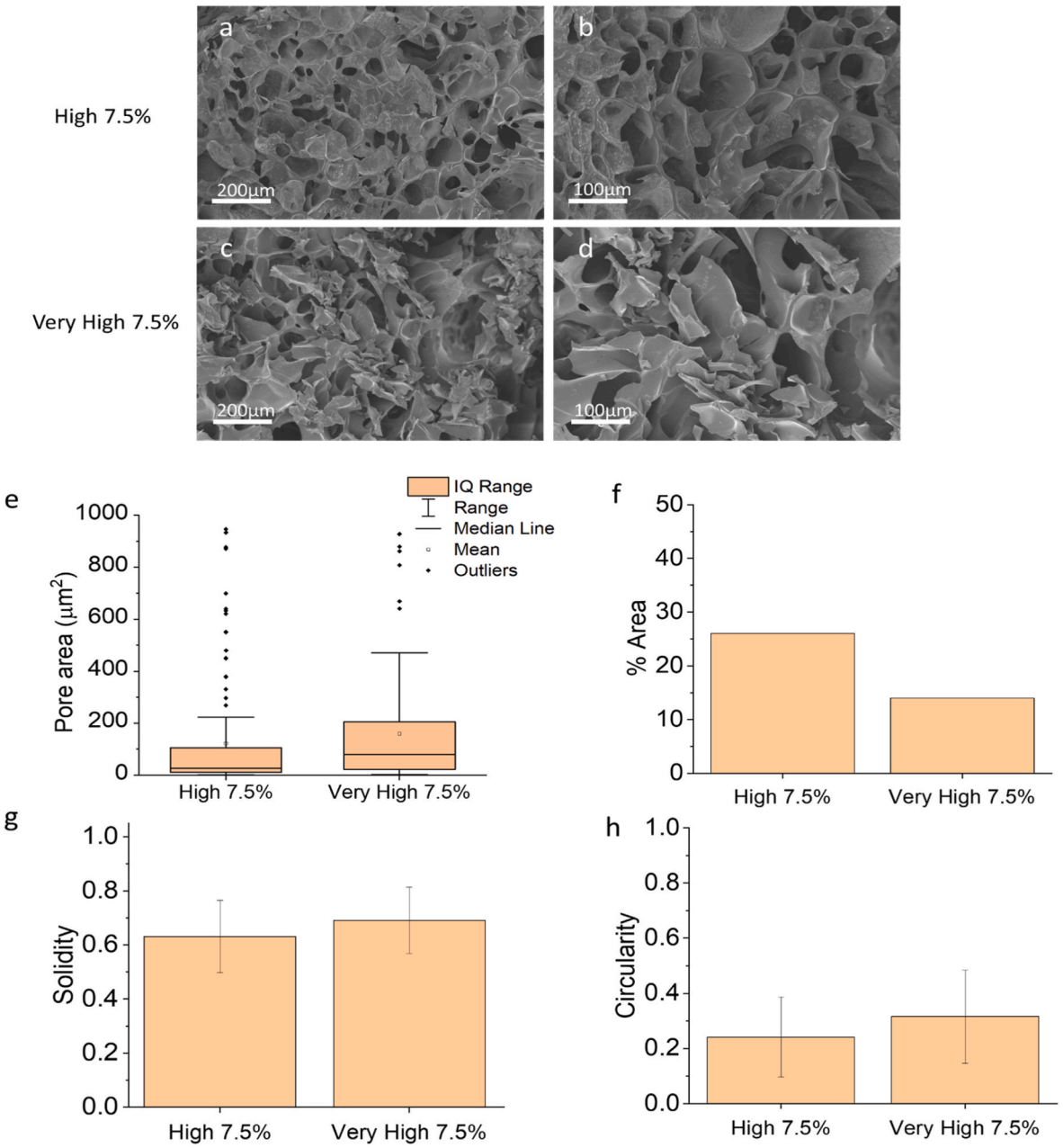

Fig. 5. SEM images of crosslinked GelMA hydrogels a) and b) show GelMA High at magnifications, respectively, of 250× an 500×, c) and d) show GelMA Very High at magnifications, respectively, of 250× an 500X e) analysis of pore area f) porosity % on the total area g) analysis of solidity h) analysis of circularity.

After these preliminary investigations, we chose GelMA High and Very High 7.5% as matrix bioinks for spheroids formation in bioprinted structures.

3.3. Scanning electron microscopy of GelMA solutions selected for 3D bioprinting

After selecting GelMA High and Very High (concentration of 7.5% w/v) as bioinks for the following 3D bioprinting step, a further investigation on microscale was carried out through Scanning Electron Microscopy (SEM) as shown in Fig. 5 a-d. To analyze and quantify the differences between the selected bioinks, ImageJ software was employed. First of all, pore area and percentage of the area occupied by porosity were estimated. Interestingly, pore area was not so different between the two formulations, as visible in Fig. 5 e. Pore area was 122 ± 212 µm^2 for High 7.5% and 160 ± 211 µm^2 for Very High 7.5%, therefore slightly larger in Very High 7.5% formulation, even if no statistical significance was witnessed. On the contrary, High 7.5% formulation showed a % of porosity of 26% and Very High 7.5% of 14% (Fig. 5 f), resulting in a denser material. This difference in density could be associated with different mechanical properties [53], with higher gel hardness and stability for Very High 7.5% formulation. The higher % of porosity of crosslinked GelMA High 7.5% could promote the exchange of nutrients and waste products during cell culture. Porosity was also analyzed in terms of solidity (**Equation (2)**, Fig. 5 g), to have an idea of the porosity jagging, and of circularity (**Equation (3)**, Fig. 5 h), where circularity = 1 describes a perfect circle. The differences between GelMa High 7.5% and Very High 7.5% in terms of these two parameters were not statistically significant, therefore, for what concerns the pore shape, the two formulations were quite equivalent.

$$Solidity = \frac{Area}{Convex\ area} \quad (2)$$

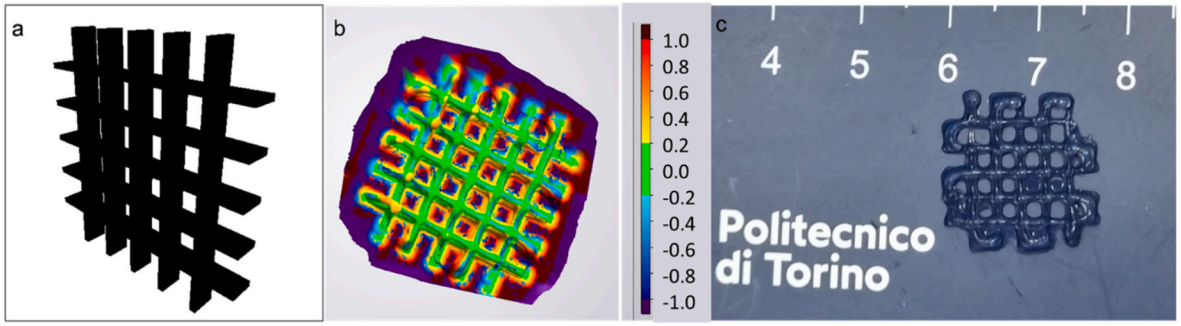

Fig. 6. a) CAD model, b) heath map (measurement unit is mm) and c) picture of crosslinked GelMA bioprinted grid architecture.

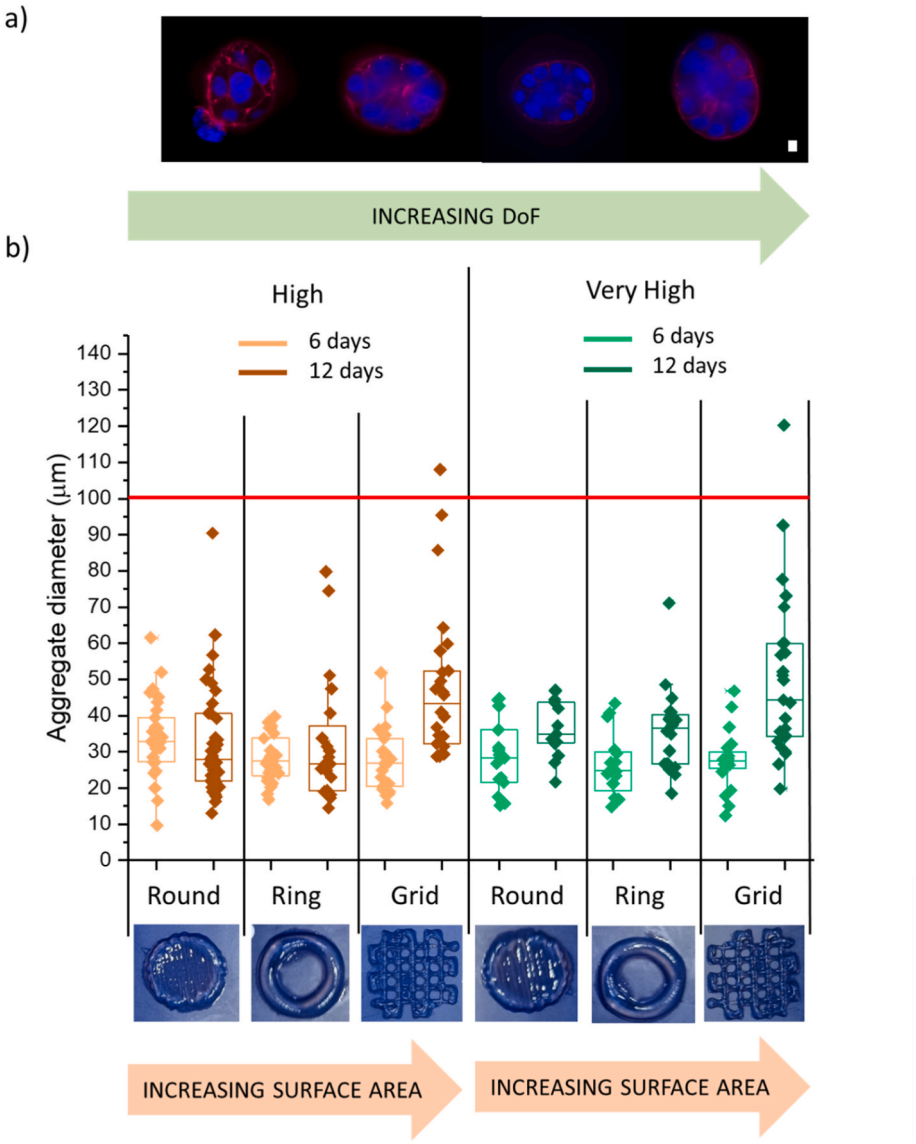

Fig. 7. a) Images of spheroids stained WGA-DAPI. Scale bar: 10 μm. Analysis of aggregates diameters measured after 6 and 12 days of culture expressed as frequency of each diameters class for crosslinked GelMA High and Very High bioprinted architecture (x-axis shows the aggregates diameter, measurement unit is μm).

$$Circularity = \frac{4 * \pi * Area}{Perimeter^2} \quad 3$$

3.4. 3D bioprinting GelMA architectures for spheroids generation

To explore the potential of the selected GelMA bioinks to produce 3D models for the study of cancer spheroids, three different architectures were designed and translated in G-code using BioCAD software

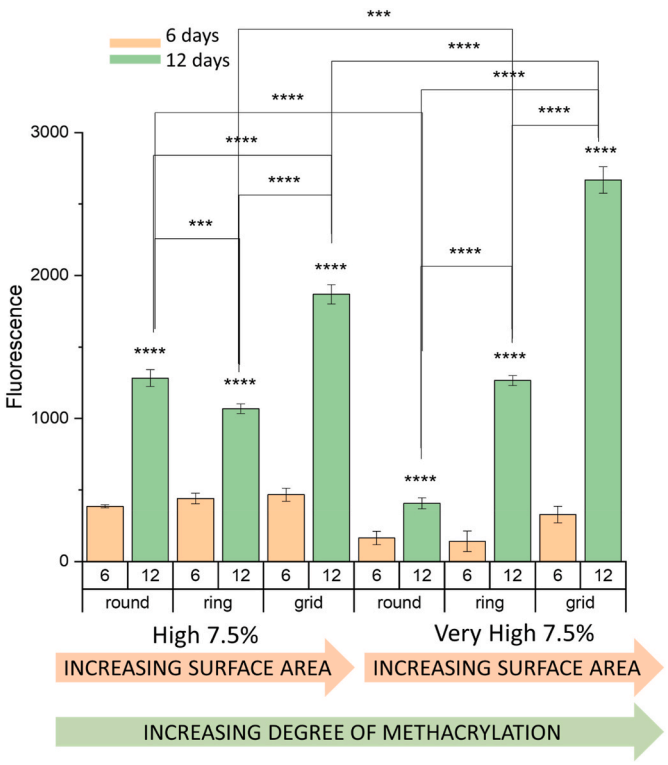

Fig. 8. Cell metabolic activity inside the different crosslinked GelMA bioprinted architectures detected at 6 and 12 days of culture. Statistical analysis was performed with two-ways ANOVA (*p < 0.05, **p < 0.01, ***p < 0.001, ****p < 0.0001).

(RegenHu, Switzerland): a circle, a ring and a grid. As reported in the Material and Methods section, all the structures were printed using the same amount of cell laden GelMA. Consequently, the three structures differ from the spatial organization of the laden cells and from the surface area exposed to culture medium, that could affect nutrients and oxygen supplying and therefore the spheroid formation and growth [54]. Surface area/volume ratio was calculated for the three geometries, resulting in 12.8 for circular architecture, 21.3 for the ring one and 49.0 for the grid one. To evaluate the shape fidelity of the bioprinted architectures (Fig. 6 c) with the CAD model (Fig. 6 a), the most complex structure, the grid, was analyzed with a 3D scanner. As appreciable in the heat map (Fig. 6 b), the discrepancies between the CAD and the printed structure were often lower than 0.2 mm (green color), which confirms the good printability of these GelMA bioinks.

3.5. *Evaluation of spheroid formation and evolution in the bioprinted architectures*

To follow the growth of cell aggregates in bioprinted systems, cells and aggregate diameters were analyzed using the confocal fluorescence microscopy, after 6 and 12 days of culture. The samples were fixed and stained with wheat germ agglutinin (WGA) Alexa fluor 647 conjugated, which binds to sialic acid and *N*-acetylglucosaminyl residues, resulting in a cell surface staining, allowing the measurement of cells and aggregates diameters (Fig. 7 a).

As shown in Fig. 7 b, which reports the aggregates' diameters of each material in each configuration, over time a slight increase in size diameter (at least in the higher diameters) was observed in all the samples, with similar trends in both High and Very High formulations. However, grid architecture supported the growth of aggregates with higher diameters, with elements that exceeded the 100 μm at 12 days. Crosslinked GelMA Very High in grid configuration shows spheroids with the highest diameters. Similarly, also in ring architecture an increasing trend was observed in both High and Very High formulations. The higher spheroids dimensions in grid architecture could be ascribable to the better exchange of oxygen and nutrients, due to the higher surface area exposed to the cell culture medium (grid > ring > round). For this reason, 3D bioprinting and the possibility to have different geometries is a crucial tool to be able to tune cancer cell behavior.

Only the grid architecture was able to give rise to cell aggregates definable as spheroids, which indeed display a diameter >100 μm [23]. However, considering the increase of aggregates size over time in the other two architectures, we could suppose that they do not prevent spheroid formation, but maybe need more time to allow aggregates growing. With the right geometry, both High and Very High GelMA 7.5% formulation could be considered good bioinks, in which to explore the spheroid formation and evolution.

To elucidate differences between GelMA formulations and architectures in terms of cellular metabolic activity, Resazurin assay was performed. This test allows to check cell metabolic activity inside the bioprinted samples and, not requiring cell lysis, to monitor the growth kinetics at different times. Fig. 8 displays cell metabolic activity inside the different architectures checked at 6 and 12 days.

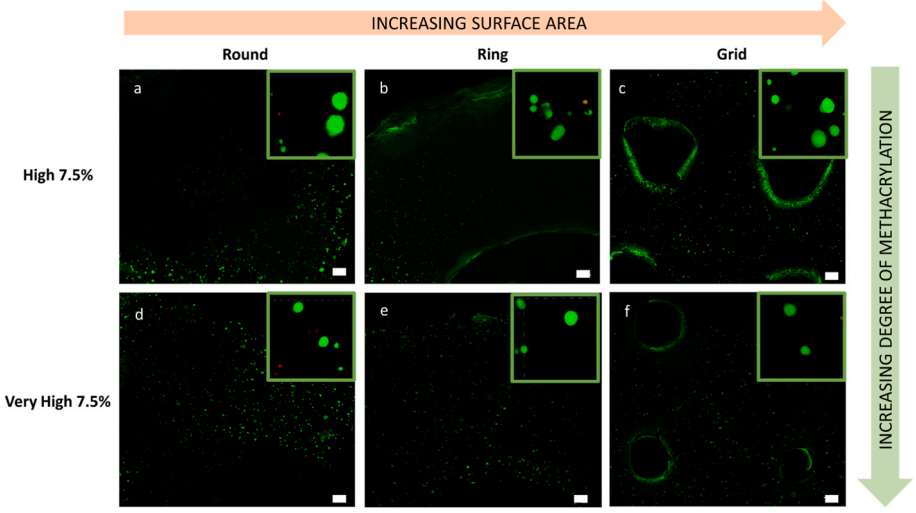

Fig. 9. Fluorescent images of LIVE/DEAD assays of A549 cells after 12 days of cultures in the 3D bioprinted architectures. Scale bar: 100 μm. Green squares represent 3D z-stack confocal microscopy reconstructions of representative spheroids. Squares are 200 μm × 200 μm.

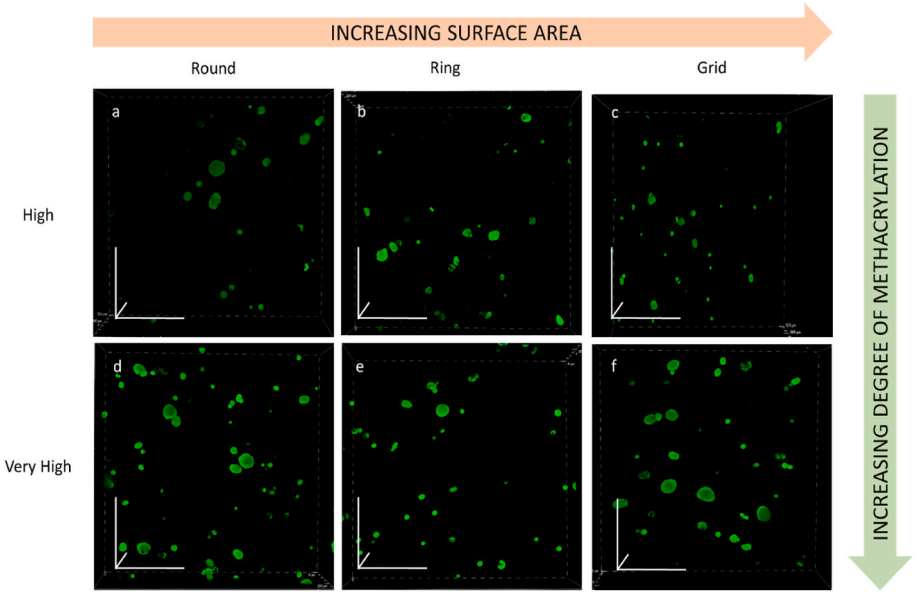

Fig. 10. 3D z-stack confocal microscopy reconstructions of sample sections coloured with LIVE/DEAD assay and imaged after 18 days of culture. Scale bar: 200 μm.

The results are in good agreement with the WGA-DAPI investigation. In fact, compared to round and ring architectures, the grid showed the highest extent of cell growth in both crosslinked GelMA hydrogels (High and Very High). In particular, from this analysis emerged that A549 cells, if in the grid architecture, prefer the most methacrylate GelMA with a statistically higher cell metabolic activity in the Very High formulation compared to the High ones after 12 days ($p < 0.0001$). Moreover, a wider difference between round and ring architectures was detectable in Very High 7.5% formulation and cell metabolic activity in the bulk round architecture was higher in High 7.5% formulation.

To obtain a qualitative analysis of the cell viability, live and dead assay after 12 days of culture was performed in all architectures and formulations. As clearly visible in Fig. 9, this assay confirms that the differences in the cell growth are not related to a higher mortality (vitality>95%), but to a different extent of cell growth in the different samples (grid > rings > round). Indeed, these images showed that almost all the cells displayed the green-fluorescent calcein-AM signal, which discriminates the live cells from the red stained dead cells. This data further confirmed that GelMA 7.5% is an optimal concentration to synthesize bioinks for cell culture experiments, both with High and Very High degree of methacrylation. In fact, the lack of dead cells inside the bioprinted architectures proves that this kind of matrices are suitable to sustain the cell growth in 3D model with good dimensions, considering the thickness of our bio printed structure of 2 mm.

In addition, again this data suggests that the system could continue to grow over time, generating bigger and viable spheroids after a longer time of culture.

To investigate the possibility to perform a longer culture without decreases in terms of cell viability, the 3D printed constructs were cultured for 18 days. Focusing on the signal from the single spheroids, we didn't observe any clues of lack of nutrient, indicating that at this time point, oxygen and nutrients were able to reach the core of these aggregates (Fig. 10). Moreover, it is possible to qualitatively observe that after 18 days of culture, crosslinked GelMA Very High shows more and bigger spheroids than High formulations.

4. Discussion

This study aimed to exploit the versatility of GelMA and its advantages in terms of biocompatibility and printability [37], to develop a 3D *in vitro* platform for the formation and culture of NSCLC spheroids. This can be of particular interest in the field of drugs and therapies screening, since spheroids are nowadays considered a promising method to improve cell viability and metabolic activity, to facilitate cell-cell interactions and to induce the release of signaling molecules close to the *in vivo* environment [11].

The first tests aimed to select from one side the right initial cell concentration and from the other side the right GelMA matrix, in terms of both DoFs and concentration % w/v. As expected, too low cell concentrations do not allow the formation of aggregates and spheroids [55] and the best concentration was 3×10^5 cells/ml. It has to be highlighted that in this study the spheroid formation and growth was evaluated not only exploring different GelMA concentrations, as in other studies [42], but also varying GelMA degree of methacrylation, which could play a pivotal role in the cellular behavior.

From the matrix side, it has been hypothesized that matrix methacrylation and porosity play a driving role in spheroid formation. Indeed, the highest concentrated and methacrylated GelMA formulations (High and Very High 10%) probably made spheroid expansion difficult. On the contrary, GelMA Medium 7.5% and 10% were not able to constrain the cells to grow in aggregates, allowing in some cases the sedimentation. Considering these results, we chose GelMA High and Very High 7.5% as matrix bioinks for spheroids formation in bioprinted structures.

After the 3D bioprinting, spheroids formation and growth were monitored. From the experiments emerged that only grid architecture was able to give rise to cell aggregates which can be consider spheroids in terms of dimensions [23]. Noteworthy, considering the increase of aggregates size over time in the other two architectures, they may need more time to allow aggregates to evolve in spheroids. As discussed in the Results part as well, Singh et al. [23] reported that spheroids of large dimensions (>400 μm) are not suitable for drug toxicity studies while spheroids of size approximately 150–350 μm can produce more reliable and reproducible data.

GelMA Very High 7.5% in grid configuration presented spheroids with the highest diameters. Another important result was in terms of cell metabolic activity: GelMA Very High 7.5% not only displayed a statistically higher cell metabolic activity in grid configuration at 12 days, but also a huge difference in cell metabolic activity trends between round and ring configuration. Moreover, in GelMA High 7.5% cell metabolic activity in round architecture was higher than in Very High 7.5%, same geometry. To better understand this behavior, we also observed SEM

images and analyzed the porosity. We supposed that in general GelMA Very High 7.5% supports better spheroids growth due to the higher density, but that the lower % of porosity results in the hindering of nutrient. On the contrary, the higher percentage of porosity in GelMA High 7.5% could be able to let nutrients enter the structure more easily, feeding also spheroid in the core of the bulk round architecture. This means that to exploit the great potential of GelMA Very High in terms of spheroid growth support, we have to play with the geometry, exposing to nutrients the highest amount of surface area possible. For this reason, 3D bioprinting is an essential tool to develop this novel platform, in order to be able to reproduce the architecture that performs better.

5. Conclusions

To conclude, a 3D *in vitro* model of NSCLC has been developed. In the constructs, cells give rise to spheroids that, as mentioned before, better mimic the *in vivo* environment. This has been possible playing with four main parameters: cell concentration, GelMA methacrylation degree, GelMA concentration and geometry. This gives the researcher the possibility to tune the properties of the system to obtain the conditions desired. Moreover, this systematic analysis and combination of various parameters could be used as model to investigate the best solution also in in vitro models of other tissues and organs.

In the future it would be of interest to both culture the models for longer time to increase spheroid dimensions and to add one of the most important components that is missing in the depicted model: the stroma. Indeed, the crosstalk between the tumor cells and the stroma would reveal interactions which would enhance the similarity between the model and the *in vivo* environment [10].

CRediT authorship contribution statement

Simona Villata: Methodology, Data curation. **Marta Canta:** Investigation, Conceptualization. **Désirée Baruffaldi:** Writing – original draft, Validation. **Ignazio Roppolo:** Investigation, Reviewing. **Candido Fabrizio Pirri:** Funding acquisition, Supervision. **Francesca Frascella:** Supervision, Writing – review & editing.

Declaration of competing interest

The authors declare that they have no known competing financial interests or personal relationships that could have appeared to influence the work reported in this paper.

Data availability

Data will be made available on request.

Acknowledgments

The authors would like to thank Paula Bosch and Alejandro Murillo, ICTP-CSIC Madrid for their support in the H^1-NMR analyses. This work was partially performed thanks to the financial support of PNC D3-4H Health Digital Driven Diagnostics, prognostics and therapeutics for sustainable Health care.

Appendix A. Supplementary data

Supplementary data to this article can be found online at https://doi.org/10.1016/j.bprint.2023.e00310.

References

[1] K. Zarogoulidis, P. Zarogoulidis, K. Darwiche, E. Boutsikou, N. Machairiotis, K. Tsakiridis, N. Katsikogiannis, I. Kougioumtzi, I. Karapantzos, H. Huang, D. Spyratos, Treatment of non-small cell lung cancer (NSCLC), J. Thorac. Dis. 5 (2013), https://doi.org/10.3978/j.issn.2072-1439.2013.07.10.

[2] A.P. Kishor Ganti, F.W. Grannis Jr., T.M. Jahan, M. Jahanzeb, S. Jude, A. Kessinger, I.T. Lennes, B.W. Loo Jr., R. Martins, G.A. Otterson, J.D. Patel, R.H. Lurie, M. C. Pinder-Schenck, K.M. Pisters, K. Reckamp, G.J. Riely, E. Rohren, S.J. Swanson, C.E. Center Douglas Wood, S.C. Yang, K.M. Gregory, M. Hughes, Non-Small Cell Lung Cancer NCCN Guidelines ® the Primary Risk Factor for Lung Cancer Is Smoking To-bacco, Which Accounts for More than 85% to 90% of NCCN Non-small Cell Lung Cancer Panel Members, 2012.

[3] S.Z. Ramadan, Methods used in computer-aided diagnosis for breast cancer detection using mammograms: a review, J. Healthc Eng. 2020 (2020), https://doi.org/10.1155/2020/9162464.

[4] C. Almeida-Ferreira, R. Silva-Teixeira, M. Laranjo, N. Almeida, G. Brites, J. Dias-Ferreira, I. Marques, R. Neves, B. Serambeque, R. Teixo, A.M. Abrantes, F. Caramelo, M.F. Botelho, Open-air cold plasma device leads to selective tumor cell cytotoxicity. https://doi.org/10.3390/app, 2021.

[5] Z. Li, S.A. Langhans, In vivo and ex vivo pediatric brain tumor models: an overview, Front. Oncol. 11 (2021), https://doi.org/10.3389/fonc.2021.620831.

[6] F. Chen, H. Hong, Y. Zhang, H.F. Valdovinos, S. Shi, G.S. Kwon, C.P. Theuer, T. E. Barnhart, W. Cai, In vivo tumor targeting and image-guided drug delivery with antibody-conjugated, radiolabeled mesoporous silica nanoparticles, ACS Nano 7 (2013) 9027–9039, https://doi.org/10.1021/nn403617j.

[7] L. Tirinato, V. Onesto, D. Garcia-Calderon, F. Pagliari, M.F. Spadea, J. Seco, F. Gentile, Human lung-cancer-cell radioresistance investigated through 2D network topology, Sci. Rep. 12 (2022), https://doi.org/10.1038/s41598-022-17018-0.

[8] J.J. Chung, H. Im, S.H. Kim, J.W. Park, Y. Jung, Toward biomimetic scaffolds for tissue engineering: 3D printing techniques in regenerative medicine, Front. Bioeng. Biotechnol. 8 (2020), https://doi.org/10.3389/fbioe.2020.586406.

[9] M. Zanon, A. Chiappone, N. Garino, M. Canta, F. Frascella, M. Hakkarainen, C. F. Pirri, M. Sangermano, Microwave-assisted methacrylation of chitosan for 3D printable hydrogels in tissue engineering, Mater. Adv. 3 (2022) 514–525, https://doi.org/10.1039/d1ma00765c.

[10] J.M. Rozenberg, G.I. Filkov, A.v. Trofimenko, E.A. Karpulevich, V.D. Parshin, V. v. Royuk, M.I. Sekacheva, M.O. Durymanov, Biomedical applications of non-small cell lung cancer spheroids, Front. Oncol. 11 (2021), https://doi.org/10.3389/fonc.2021.791069.

[11] B. Pinto, A.C. Henriques, P.M.A. Silva, H. Bousbaa, Three-dimensional spheroids as in vitro preclinical models for cancer research, Pharmaceutics 12 (2020) 1–38, https://doi.org/10.3390/pharmaceutics12121186.

[12] N.E. Ryu, S.H. Lee, H. Park, Spheroid culture system methods and applications for mesenchymal stem cells, Cells 8 (2019), https://doi.org/10.3390/cells8121620.

[13] L. Guillaume, L. Rigal, J. Fehrenbach, C. Severac, B. Ducommun, V. Lobjois, Characterization of the physical properties of tumor-derived spheroids reveals critical insights for pre-clinical studies, Sci. Rep. 9 (2019), https://doi.org/10.1038/s41598-019-43090-0.

[14] D. Lee, C. Cha, Cell subtype-dependent formation of breast tumor spheroids and their variable responses to chemotherapeutics within microfluidics-generated 3D microgels with tunable mechanics, Mater. Sci. Eng. C 112 (2020), https://doi.org/10.1016/j.msec.2020.110932.

[15] J. Kim, B.K. Koo, J.A. Knoblich, Human organoids: model systems for human biology and medicine, Nat. Rev. Mol. Cell Biol. 21 (2020) 571–584, https://doi.org/10.1038/s41580-020-0259-3.

[16] G. Rossi, A. Manfrin, M.P. Lutolf, Progress and potential in organoid research, Nat. Rev. Genet. 19 (2018) 671–687, https://doi.org/10.1038/s41576-018-0051-9.

[17] B.L. LeSavage, R.A. Suhar, N. Broguiere, M.P. Lutolf, S.C. Heilshorn, Next-generation cancer organoids, Nat. Mater. 21 (2022) 143–159, https://doi.org/10.1038/s41563-021-01057-5.

[18] A.J. Miller, B.R. Dye, D. Ferrer-Torres, D.R. Hill, A.W. Overeem, L.D. Shea, J. R. Spence, Generation of lung organoids from human pluripotent stem cells in vitro, Nat. Protoc. 14 (2019) 518–540, https://doi.org/10.1038/s41596-018-0104-8.

[19] M. Dey, I.T. Ozbolat, 3D bioprinting of cells, tissues and organs, Sci. Rep. 10 (2020), https://doi.org/10.1038/s41598-020-70086-y.

[20] D. Baruffaldi, C.F. Pirri, F. Frascella, 3D bioprinting of cell-laden carbopol bioinks, Bioprinting 22 (2021), https://doi.org/10.1016/j.bprint.2021.e00135.

[21] M. Kapałczyńska, T. Kolenda, W. Przybyła, M. Zajączkowska, A. Teresiak, V. Filas, M. Ibbs, R. Bliźniak, Ł. Łuczewski, K. Lamperska, 2D and 3D cell cultures – a comparison of different types of cancer cell cultures, Arch. Med. Sci. 14 (2018) 910–919, https://doi.org/10.5114/aoms.2016.63743.

[22] R.C. Hubrecht, E. Carter, The 3Rs and humane experimental technique: implementing change, Animals 9 (2019), https://doi.org/10.3390/ani9100754.

[23] A. Singh, P. Tayalia, Three-dimensional cryogel matrix for spheroid formation and anti-cancer drug screening, J. Biomed. Mater. Res. 108 (2020) 365–376, https://doi.org/10.1002/jbm.a.36822.

[24] X. Cui, S. Dini, S. Dai, J. Bi, B.J. Binder, J.E.F. Green, H. Zhang, A mechanistic study on tumour spheroid formation in thermosensitive hydrogels: experiments and mathematical modelling, RSC Adv. 6 (2016) 73282–73291, https://doi.org/10.1039/c6ra11699j.

[25] D. Baruffaldi, G. Palmara, C. Pirri, F. Frascella, 3D cell culture: recent development in materials with tunable stiffness, ACS Appl. Bio Mater. 4 (2021) 2233–2250, https://doi.org/10.1021/acsabm.0c01472.

[26] T. Jiang, J. Zhao, S. Yu, Z. Mao, C. Gao, Y. Zhu, C. Mao, L. Zheng, Untangling the response of bone tumor cells and bone forming cells to matrix stiffness and adhesion ligand density by means of hydrogels, Biomaterials 188 (2019) 130–143, https://doi.org/10.1016/j.biomaterials.2018.10.015.

[27] M. Petretta, S. Villata, M.P. Scozzaro, L. Roseti, M. Favero, L. Napione, F. Frascella, C.F. Pirri, B. Grigolo, E. Olivotto, In vitro synovial membrane 3D model developed

by volumetric extrusion bioprinting, Appl. Sci. 13 (2023) 1889, https://doi.org/10.3390/app13031889.
[28] J. Pape, M. Emberton, U. Cheema, 3D cancer models: the need for a complex stroma, compartmentalization and stiffness, Front. Bioeng. Biotechnol. 9 (2021), https://doi.org/10.3389/fbioe.2021.660502.
[29] K. Tanner, M.M. Gottesman, Beyond 3D culture models of cancer, Sci. Transl. Med. 7 (2015), https://doi.org/10.1126/scitranslmed.3009367.
[30] S. Swaminathan, Q. Hamid, W. Sun, A.M. Clyne, Bioprinting of 3D breast epithelial spheroids for human cancer models, Biofabrication 11 (2019), https://doi.org/10.1088/1758-5090/aafc49.
[31] T. Jiang, J.G. Munguia-Lopez, S. Flores-Torres, J. Grant, S. Vijayakumar, A. de Leon-Rodriguez, J.M. Kinsella, Directing the self-assembly of tumour spheroids by bioprinting cellular heterogeneous models within alginate/gelatin hydrogels, Sci. Rep. 7 (2017), https://doi.org/10.1038/s41598-017-04691-9.
[32] B.H. Lee, N. Lum, L.Y. Seow, P.Q. Lim, L.P. Tan, Synthesis and characterization of types A and B gelatin methacryloyl for bioink applications, Materials 9 (2016), https://doi.org/10.3390/ma9100797.
[33] C. Kilic Bektas, V. Hasirci, Cell loaded 3D bioprinted GelMA hydrogels for corneal stroma engineering, Biomater. Sci. 8 (2020) 438–449, https://doi.org/10.1039/c9bm01236b.
[34] I. Pepelanova, K. Kruppa, T. Scheper, A. Lavrentieva, Gelatin-methacryloyl (GelMA) hydrogels with defined degree of functionalization as a versatile toolkit for 3D cell culture and extrusion bioprinting, Bioengineering 5 (2018), https://doi.org/10.3390/bioengineering5030055.
[35] K. Yue, G. Trujillo-de Santiago, M.M. Alvarez, A. Tamayol, N. Annabi, A. Khademhosseini, Synthesis, properties, and biomedical applications of gelatin methacryloyl (GelMA) hydrogels, Biomaterials 73 (2015) 254–271, https://doi.org/10.1016/j.biomaterials.2015.08.045.
[36] X. Ma, C. Yu, P. Wang, W. Xu, X. Wan, C.S.E. Lai, J. Liu, A. Koroleva-Maharajh, S. Chen, Rapid 3D bioprinting of decellularized extracellular matrix with regionally varied mechanical properties and biomimetic microarchitecture, Biomaterials 185 (2018) 310–321, https://doi.org/10.1016/j.biomaterials.2018.09.026.
[37] Y. Piao, H. You, T. Xu, H.P. Bei, I.Z. Piwko, Y.Y. Kwan, X. Zhao, Biomedical applications of gelatin methacryloyl hydrogels, Eng. Regeneration 2 (2021) 47–56, https://doi.org/10.1016/j.engreg.2021.03.002.
[38] E.M. Kim, G.M. Lee, S. Lee, S. jeong Kim, D. Lee, D.S. Yoon, J. Joo, H. Kong, H. H. Park, H. Shin, Effects of mechanical properties of gelatin methacryloyl hydrogels on encapsulated stem cell spheroids for 3D tissue engineering, Int. J. Biol. Macromol. 194 (2022) 903–913, https://doi.org/10.1016/j.ijbiomac.2021.11.145.
[39] A.A. Aldana, F. Valente, R. Dilley, B. Doyle, Development of 3D bioprinted GelMA-alginate hydrogels with tunable mechanical properties, Bioprinting 21 (2021), https://doi.org/10.1016/j.bprint.2020.e00105.
[40] X. Zhao, Q. Lang, L. Yildirimer, Z.Y. Lin, W. Cui, N. Annabi, K.W. Ng, M. R. Dokmeci, A.M. Ghaemmaghami, A. Khademhosseini, Photocrosslinkable gelatin hydrogel for epidermal tissue engineering, Adv. Healthcare Mater. 5 (2016) 108–118, https://doi.org/10.1002/adhm.201500005.
[41] S. Abdollahi Baghban, M. Ebrahimi, S. Bagheri-Khoulenjani, M. Khorasani, A highly efficient microwave-assisted synthesis of an LED-curable methacrylated gelatin for bio applications, RSC Adv. 11 (2021) 14996–15009, https://doi.org/10.1039/d1ra01269j.
[42] E. Kaemmerer, F.P.W. Melchels, B.M. Holzapfel, T. Meckel, D.W. Hutmacher, D. Loessner, Gelatine methacrylamide-based hydrogels: an alternative three-dimensional cancer cell culture system, Acta Biomater. 10 (2014) 2551–2562, https://doi.org/10.1016/j.actbio.2014.02.035.
[43] A.I. Van Den Bulcke, B. Bogdanov, N. De Rooze, E.H. Schacht, M. Cornelissen, H. Berghmans, Structural and rheological properties of methacrylamide modified gelatin hydrogels, Biomacromolecules 1 (2000) 31–38, https://doi.org/10.1021/bm990017d.
[44] K. Yue, X. Li, K. Schrobback, A. Sheikhi, N. Annabi, J. Leijten, W. Zhang, Y. S. Zhang, D.W. Hutmacher, T.J. Klein, A. Khademhosseini, Structural analysis of photocrosslinkable methacryloyl-modified protein derivatives, Biomaterials 139 (2017) 163–171, https://doi.org/10.1016/j.biomaterials.2017.04.050.
[45] M. Sutter, J. Siepmann, W.E. Hennink, W. Jiskoot, Recombinant gelatin hydrogels for the sustained release of proteins, J. Contr. Release 119 (2007) 301–312, https://doi.org/10.1016/j.jconrel.2007.03.003.
[46] L. Vretik, V. Kyrychenko, G. Smolyakov, O. Yaroshchuk, V. Zagniy, T. Gavrilko, V. Syromyatnikov, Photochemical transformations in bis-methacrylic polymers for liquid crystal photoalignment: IR spectroscopy studies, Mol. Cryst. Liq. Cryst. 536 (2011), https://doi.org/10.1080/15421406.2011.538611, 224/[456]-235/[467].
[47] S. Abdollahi Baghban, M. Ebrahimi, S. Bagheri-Khoulenjani, M. Khorasani, A highly efficient microwave-assisted synthesis of an LED-curable methacrylated gelatin for bio applications, RSC Adv. 11 (2021) 14996–15009, https://doi.org/10.1039/d1ra01269j.
[48] M. Sun, X. Sun, Z. Wang, S. Guo, G. Yu, H. Yang, Synthesis and properties of gelatin methacryloyl (GelMA) hydrogels and their recent applications in load-bearing tissue, Polymers 10 (2018), https://doi.org/10.3390/POLYM10111290.
[49] Z. Chen, F. Wang, J. Zhang, X. Sun, Y. Yan, Y. Wang, J. Ouyang, J. Zhang, T. Honore, J. Ge, Z. Gu, Study on development of composite hydrogels with tunable structures and properties for tumor-on-a-chip research, Front. Bioeng. Biotechnol. 8 (2020), https://doi.org/10.3389/fbioe.2020.611796.
[50] S. Sant, P.A. Johnston, The production of 3D tumor spheroids for cancer drug discovery, Drug Discov. Today Technol. 23 (2017) 27–36, https://doi.org/10.1016/j.ddtec.2017.03.002.
[51] J. Bomo, F. Ezan, F. Tiaho, M. Bellamri, S. Langouët, N. Theret, G. Baffet, Increasing 3D matrix rigidity strengthens proliferation and spheroid development of human liver cells in a constant growth factor environment, J. Cell. Biochem. 117 (2016) 708–720, https://doi.org/10.1002/jcb.25356.
[52] I.G. Goncalves, J.M.G. Aznar, Extracellular matrix density regulates the formation of tumour spheroids through cell migration, PLoS Comput. Biol. 17 (2021), https://doi.org/10.1371/JOURNAL.PCBI.1008764.
[53] F. Souza Almeida, K.C. Guedes Silva, A. Matias Navarrete de Toledo, A.C. Kawazoe Sato, Modulating porosity and mechanical properties of pectin hydrogels by starch addition, J. Food Sci. Technol. 58 (2021) 302–310, https://doi.org/10.1007/s13197-020-04543-x.
[54] M. Lee, B.M. Wu, J.C.Y. Dunn, Effect of scaffold architecture and pore size on smooth muscle cell growth, J. Biomed. Mater. Res. 87 (2008) 1010–1016, https://doi.org/10.1002/jbm.a.31816.
[55] G. Benton, G. DeGray, H.K. Kleinman, J. George, I. Arnaoutova, In vitro microtumors provide a physiologically predictive tool for breast cancer therapeutic screening, PLoS One 10 (2015), https://doi.org/10.1371/journal.pone.0123312.